Available online at www.garmian.edu.krd

Passer Journal

Passer 6 (Issue 1) (2024) 192-197

http://passer.garmian.edu.krd/

Effect of temperature on the reaction of pristine and Au-doped SnO_2 pyramid clusters with H_2: A transition state theory study

Mudar A. Abdulsattar[1*]

[1]*Ministry of Science and Technology, Baghdad, Iraq*

Received 23 October 2023; revised 01 April;
accepted 02 April 2024; available online 21 April 2024

DOI: 10.24271/PSR.2024.421994.1412

ABSTRACT

H_2 gas reaction with pristine and Au-doped SnO_2 clusters is calculated and compared with the experiment. A new generalized version of the Evans–Polanyi principle is employed. As a function of temperature, the transition state is used to calculate the activation of Gibbs free energy, including its components enthalpy and entropy. H_2 autoignition at elevated temperatures is considered using logistic functions. Reaction rate, response, response time, and recovery time are calculated and compared with the experiment. Results show a strong temperature dependence of H_2 reactions, while O_2 recovery reactions depend on temperature through the change of activation energy only. Promising results that need more comparisons between experiment and theory are obtained to validate the new formalism.

Keywords: Au Doping; Sno₂ Cluster; H₂ Gas Sensor; Density Functional Theory; Transition State; Activation Entropy; Gibbs Energy.

1. Introduction

Transition state theory[1,2] is one of the leading methods for calculating chemical substances' reaction rates. It has been widely used since its proposal began in the previous century[3]. In this theory, a transition state with an activation energy must be overcome for the reaction to proceed. The transition state theory was applied to various reactions, including gas sensing[4,5], membranes[3], and atmospheric and combustion reactions[6].

Tin dioxide is one of the most preferred materials in gas sensing[7,8]. SnO_2 has been used to detect gases such as NH_3[9], CO[10], and NO_2[11]. One of the reasons why tin dioxide is a suitable gas sensor is the high number of oxygen vacancies at its surface[12]. The surface reconstruction of the SnO_2 nanoparticles forms pyramids that have enhanced surface area over other materials[13]. Usually, SnO_2 sensing is enhanced by doping with specific amounts of catalysts such as Pt, Au, and Ag. Catalysts decrease the activation energy needed to be overcome so that the reaction between the gas and the sensor can proceed faster.

Hydrogen is one of the most important gases in industry. It is used as a clean energy carrier[14], petrochemistry[15], hydrogenation[16], coolant[17], and semiconductor manufacturing. The detection of H_2 is vital since it can form explosive mixtures with air at small ratios as low as 4%. Hydrogen autoignition temperature is at 536 ℃[18].

* Corresponding author
E-mail address: mudarahmed3@yahoo.com (Instructor).
Peer-reviewed under the responsibility of the University of Garmian.

Theoretical simulation of gas sensors is usually performed using density functional theory (DFT)[19,20]. This theory allows for the determination of several quantities that are related to the gas-sensing mechanism. The quantities include energy gap[21], reaction rate[22], response and recovery times[19]. One of the problems in using DFT is the size of calculations, especially after doping. The number of atoms included in DFT calculations usually doesn't exceed 100 or several hundred atoms. However, this is overcome because the interaction between atoms doesn't need more than including three or four neighbors to be in nearly correct calculations.

Another problem is the ratio of dopant to doped materials. Since the number of atoms to be considered in DFT calculations is limited to 100 or several hundreds of atoms, the small doping ratio of one atom to 10000 (for example) atoms is challenging in DFT calculations. This problem is solved using the Evans–Polanyi principle to interpolate or extrapolate the required ratio[23]. The Evans–Polanyi principle is usually limited to Arrhenius-type reactions. However, the Evans–Polanyi principle has been generalized to be used in transition state theory by introducing a modified principle[4].

In the present work, the sensitivity of pristine and Au-doped SnO_2 clusters to H_2 gas concentration is calculated using DFT and transition state theory as a function of temperature. A newly modified Evans–Polanyi principle obtains activation energies for different doping ratios by interpolating previous theoretical or experimental reference reactions. The autoignition temperature of H_2 is considered using logistic functions. Oxygen recovery

reaction is also calculated. Comparison with experimental results is performed whenever such results are available.

2. Theory

The Gaussian 09 computational chemistry program performs present calculations[24]. DFT is used at the B3LYP level with a 6-311G** basis set for light atoms and SDD functionals for heavy atoms. Dispersion corrections at the GD3BJ level are included because of their importance in gas sensing calculations[25]. The B3LYP/6-311G** method and basis set are successfully used in gas sensing calculations[25], while dispersion correction is necessary since induced dipole reactions are a dominant component of the H_2 and O_2 homomolecules' reaction mechanism.

SnO_2 pyramids were successfully used previously in gas sensor calculations. These pyramids are found at the surface of pristine and doped SnO_2 structures[13]. Fig. 1a shows a SnO_2 pyramid with an H_2 molecule adsorbed on its surface compared to a doped Au/SnO_2 cluster with an H_2 molecule adsorbed on its surface.

The general equation that can give the reaction between Au/SnO2 with adsorbed hydrogen molecules[4]:

$$\frac{d[Au/SnO_2]}{dt} = -[Au/SnO_2]^u\,[H_2]_e^v\,k(T), \quad (1)$$

$$k(T) = A\ T^m \exp\left(\frac{-\Delta G^{\ddagger}}{k_B T}\right). \quad (2)$$

In the above equations, $[Au/SnO_2]$ and $[H_2]$ are the Au-doped SnO_2 clusters and H_2 molecule concentrations. The powers (u) and (v) on the concentrations in Eq. (1) can be given the value 1 for slight variations in the concentrations. The subscript (e) in the H_2 concentration indicates that the effective concentration of hydrogen is used since H_2 reacts with the oxygen in the air simultaneously as it approaches its autoignition temperature at 536 ℃[18], as illustrated later. k(T) is the reaction rate constant that does not depend on reactant concentrations. k(T) is a function of temperature (T) and the Gibbs free energy of activation ($\Delta G^{\ddagger}$). Gibbs free energy is also a function of temperature, enthalpy (H), and entropy (S):

$$G = H - TS \quad (3)$$

For closely related reactions in gas sensing, activation energy is usually obtained using Evans–Polanyi principle as a function of enthalpy of reaction[23]:

$$E_a = E_0 + \alpha \Delta H \quad (4)$$

In the above equation, E_0 and α are parameters that are fit to reference experiments. However, this equation cannot be applied directly to transition state theory since the equations of this theory, such as Eq. (2), depend on Gibbs free energy of activation rather than enthalpy. A recent suggestion is a modified Evans–Polanyi principle that relates closely related reactions by the equation[4]:

$$\Delta G^{\ddagger} = \Delta G_0^{\ddagger} + \beta \Delta G \quad (5)$$

In the above equation, $\Delta G^{\ddagger}$ is Gibbs free energy of transition. $\Delta G_0^{\ddagger}$, β, and ΔG are fitting parameters to previous reference experimental or theoretical values results for Gibbs free energy of transition. Eq. (5) is compatible with Eq. (2) for the transition state theory. In addition, Eq. (5) includes the effect of entropy and temperature, which are components of Gibbs free energy, as in Eq. (3).

In Eq. (1), the concentration of hydrogen is given as the effective concentration $[H_2]_e$. An effective concentration of H_2 is used because hydrogen reacts with oxygen in air. This reaction becomes spontaneous as H_2 reaches its autoignition temperature at 536 ℃[18]. In the case of the reaction of H_2 with oxygen in the air, the material used as a sensor (SnO_2) will not feel sensitive to H_2 since the material's oxygen content is unchanged. To take the H_2 autoignition effect into account, a logistic function is used as in the equation:

$$f(T) = \frac{1}{1+e^{k_s(T-T_0)}} \quad (6)$$

In the above equation, k_s is the steepness of the decrease in hydrogen concentration, while T_0 is the temperature at which H_2 reaches half of its original concentration. In the present case, to account for the burning of H_2 near autoignition temperature at 536 ℃, the k_s value is 0.04 K^{-1}, and T_0 is 480 ℃.

The sensitivity or response of a sensor is defined as the ratio of the resistance in air (Ra) to that of the resistance in the existence of the detected gas (R_a/R_g). This response or sensitivity is proportional to the reaction rate. For the Au-doped SnO_2 pyramid, the equation is:

$$\text{Response(theoretical)} = C\left|\frac{d[Au/SnO_2]}{dt}\right| \quad (7)$$

In the above equation, an absolute value is used because the number of Au/SnO_2 pyramids decreases when interacting with hydrogen to produce $AuSn_9O_{14}$ pyramids as in Eq. (8). C is a proportionality constant that correlates the number of reactions to the response.

One of the crucial results of gas sensing experiments is the response time and recovery time. These two measured timings are important in gas sensor real-life applications. These are defined as the sensor resistivity reaching 90% of its steady state. Integrating Eq. (1), the 90% response time is given by:

$$t_{res(90\%)} = \frac{\ln(10)}{[H2]_e\,A\,T^m \exp\left(\frac{-G^{\ddagger}}{k_B T}\right)} \quad (8)$$

The 90% recovery is defined as the time needed to recover (oxidize) 90% of oxygen-deficient clusters as in the equation:

$$t_{rec(90\%)} = \frac{\ln(10)}{[O_2]_e\,A\,T^m \exp\left(\frac{-G^{\ddagger}}{k_B T}\right)} \quad (9)$$

3. Results and discussion

Fig. 1 shows the adsorption of H_2 at the surface of the SnO_2 pyramid (Fig. 1a) and Au/SnO_2 pyramid (Fig. 1b). These adsorption states can be labeled $[SnO_2\text{---}H_2]^v$ and $[Au/SnO_2\text{---}H_2]^v$ respectively. The (v) in these labels refers to adsorption via van der Waals forces. As seen in Fig. 1b, the shape of the Au/SnO_2 pyramid is altered because of the difference in the most

favorable oxidation state between Sn (+4) and Au (+3). Although the H_2 molecule does not have a dipole moment, an induced dipole moment is formed in this molecule due to interaction with dipole charges of SnO_2 or Au/SnO_2 pyramids.

Fig. 2 shows the transition state of the interaction of H_2 with the SnO_2 pyramid (Fig. 2a) and Au/SnO_2 pyramid (Fig. 2b). These transition states are labeled $[SnO_2\text{---}H_2]^{\ddagger}$ and $[Au/SnO_2\text{---}H_2]^{\ddagger}$ respectively. The transition state has the highest potential energy along the reaction path. The first step in the interaction of H_2 with the two materials is the adsorption on the surface, as in Fig. 1. After that, the H_2 molecule vibrations make this molecule interact with oxygen in the SnO_2 pyramid or Au/SnO_2 pyramid. The results of interaction are (at 25 ℃):

$$Sn_{10}O_{16}+H_2 \rightarrow Sn_{10}O_{15}+H_2O \ (\Delta G= -1.375 \text{ eV}), \quad (10)$$

$$AuSn_9O_{15}+H_2 \rightarrow AuSn_9O_{14}+H_2O \quad (\Delta G= -1.250 \text{ eV}). \quad (11)$$

In the above two equations, ΔG is the Gibbs free energy of the reaction. The negative value of ΔG is an indication that the reaction is spontaneous.

The number of moles of Au for total moles of the sum of (Au and SnO_2 moles) in the $AuSn_9O_{15}$ cluster is 1/10 or 10%. Experimentally, this high ratio exceeds the optimum percentage needed for high-sensitivity gas sensors[26]. Eq. (5) is used to obtain the Gibbs free activation energy for the correct percentage of Au. Interpolation of $\Delta G^{\ddagger}$ from Fig. 3 represents the variation of $\Delta G^{\ddagger}$ for pure and Au-doped SnO_2 in various temperatures. It can be seen from Fig. 3 that $\Delta G^{\ddagger}$ of pure SnO_2 is slightly higher than that of Au-doped SnO_2 for all temperatures. Lower activation energy results in a higher reaction rate for the doped pyramid, as in Eqs. (1,2). The entropy value for the Gibbs activation energy is always negative, which explains the increase of $\Delta G^{\ddagger}$ with temperature as required by Eq. (3).

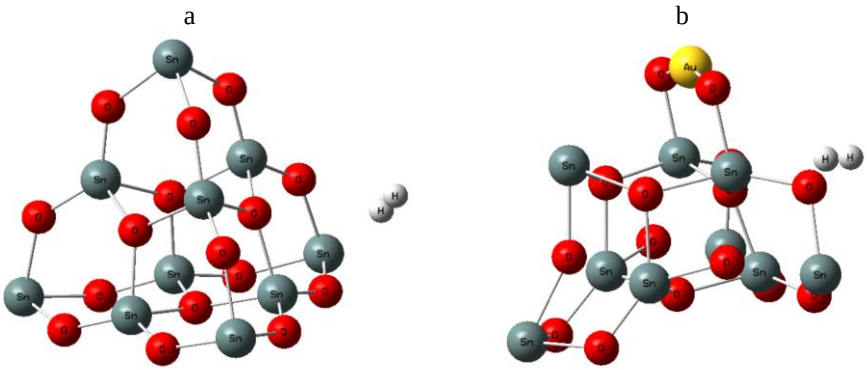

Figure. 1: (a) The optimized $Sn_{10}O_{16}$ cluster with adsorbed H_2 molecule ($[SnO_2\text{---}H_2]^{v}$); (b) optimized $AuSn_9O_{15}$ cluster with adsorbed H_2 molecule ($[Au/SnO_2\text{---}H_2]^{v}$).

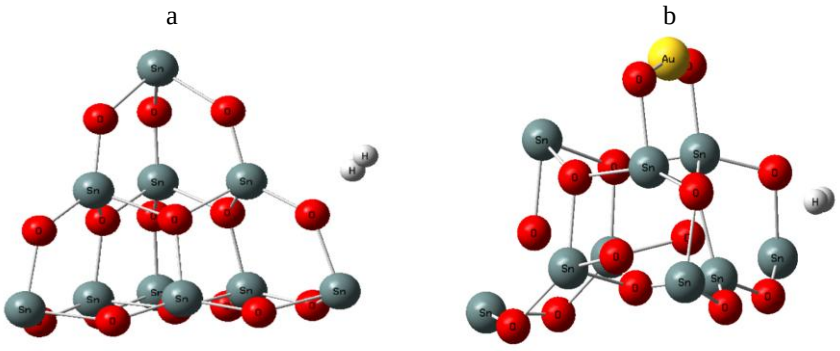

Figure. 2:. (a) The optimized transition state of $Sn_{10}O_{16}$ pyramid with H_2 molecule; (b) The optimized transition state of $AuSn_9O_{15}$ pyramid with H_2 molecule.

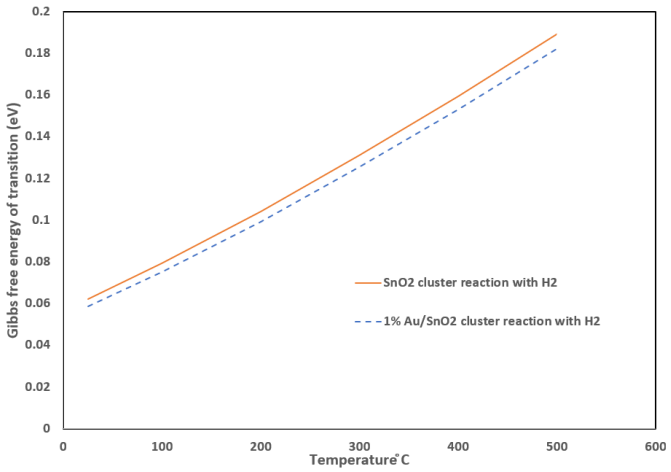

Figure. 3: Calculated Gibb free energy of transition as a function of the investigated temperatures as in Eq. (5) for the pristine and 1% (molar) Au-doped SnO_2 clusters with H_2.

Fig. 4 and 5 show the calculated response to H_2 of pure SnO_2 and 1% Au/SnO_2 compared to experimental results [26]. Both figures result from the application of Eq. (7) and the details of Eqs. (1-6). The temperature exponent (m) used in Fig. 4 and 5 is four (4), showing a high temperature dependence. The reason for high-temperature dependence is the ability of H_2 to defuse through the sensor surface to deep layers. This diffusion is strongly affected by the increase in temperature.

Fig. 6 shows the response time of Au/SnO_2 to H_2 as a function of temperature with a comparison to the experiment. The theoretical data resulted from applying Eq. (8). There was acceptable agreement between theory and experiment, especially in decreasing recovery time with the temperature increase.

Fig. 7 shows the recovery time of oxygen-deficient Au/SnO_2 as it reacts with ambient oxygen to restore 90% of the original fully oxidized Au/SnO_2 as in the equation:

$$AuSn_9O_{14}+½O_2 \rightarrow AuSn_9O_{15}\ (\Delta G=-0.722\ eV), \quad (12)$$

Eq. (5) is used to obtain the values of Gibbs free energy for the required concentration of Au in SnO_2. Fig. 7 shows good agreement between theory and experiment, including the trend of increasing recovery time with temperature. The value of temperature exponent (m) in Eq. (9) is zero (0). Temperature dependence shows that the increase in recovery time with temperature is due to the increase of $\Delta G^{\ddagger}$ with temperature only and independent of direct temperature dependence as described by the exponent m in Eq. (9).

Fig. 8 shows the differences in energy gap, HOMO (highest occupied molecular orbital), LUMO (lowest unoccupied molecular orbital), and Fermi levels between pristine SnO_2 and Au-doped SnO_2. The calculated energy gap of the SnO_2 pyramid is 3.876 eV compared to the Au-doped gap of 1.619 eV. The high electron affinity of Au compared to the Sn atom attracts electrons to the Au site, forming energy levels inside the original SnO_2 gap. The decrease of the gap is manifested by the Fermi levels of SnO_2 [27] and Au [28] included in Fig. 8. Analyzing charges in Fig. 1b for the adsorption of H_2 molecule using natural bond order (NBO) results in Sn charges in the range 1.4 to 2.5 atomic units of charge (a.u.) depending on the position of the Sn atom. Au atom has a 0.638 (a.u.) charge due to its deep Fermi level at 5.51 eV, which induces electron transfer to the Au atom from surrounding atoms. Oxygen atoms have a charge range of -1.24 to -1.35 (a.u.) except for the oxygen atoms near the Au atom, which has -0.91 (a.u.) due to the high oxidation resistance of gold and deep Au Fermi level. Finally, the initially neutral hydrogen atoms have the two induced charges 0.01 and -0.01 due to interaction with the Au/SnO_2 pyramid.

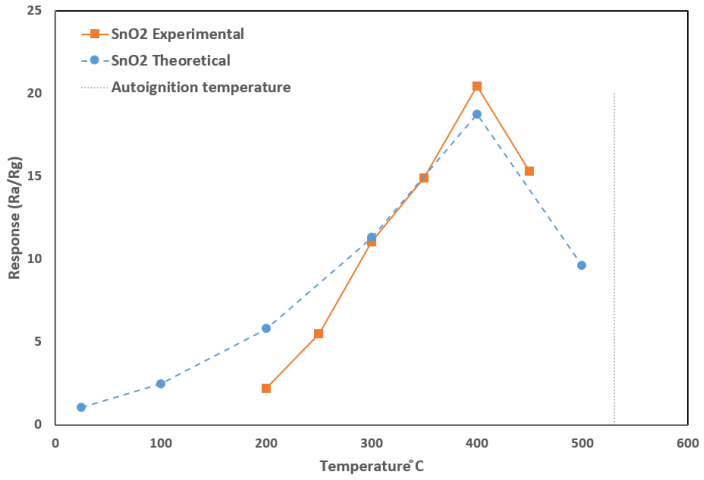

Figure. 4:. The experimental [26] and theoretical responses of the SnO_2 sensor to 5000 ppm H_2 gas at different temperatures.

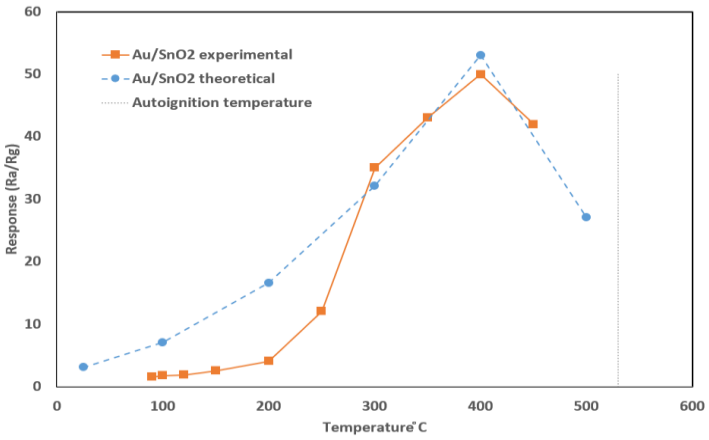

Figure. 5:. The experimental [26] and theoretical responses of 1% Au/SnO_2 (molar) sensor to 5000 ppm H_2 gas at different temperatures.

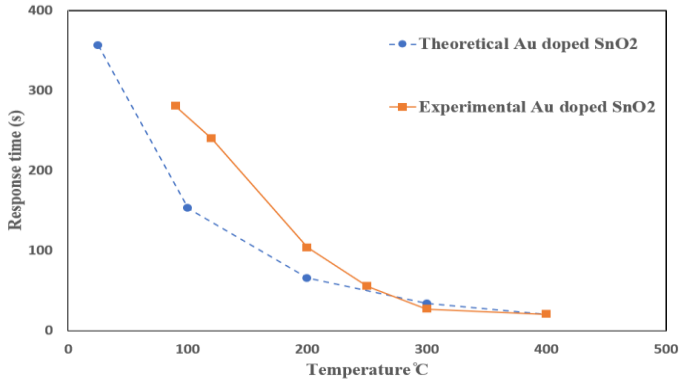

Figure. 6:. Theoretical and experimental response time of 1% Au doped SnO_2 (molar) pyramid to 5000 ppm H_2 as a function of temperature. Experimental results are from reference [26].

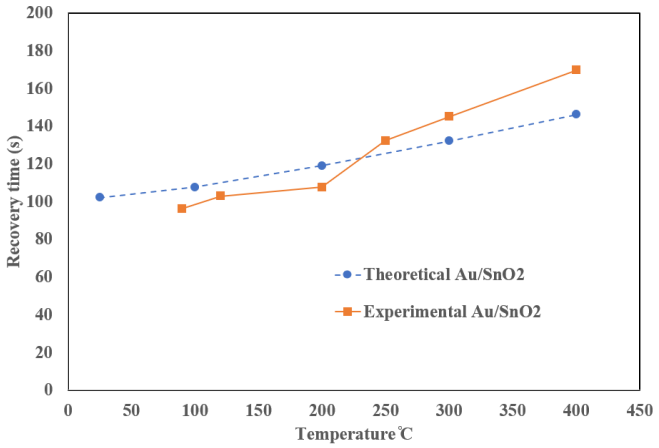

Figure. 7:. Shows the theoretical and experimental recovery time of 1% Au doped (molar) SnO_2 pyramid to 5000 ppm H_2 as a function of temperature. Experimental results are from reference [26].

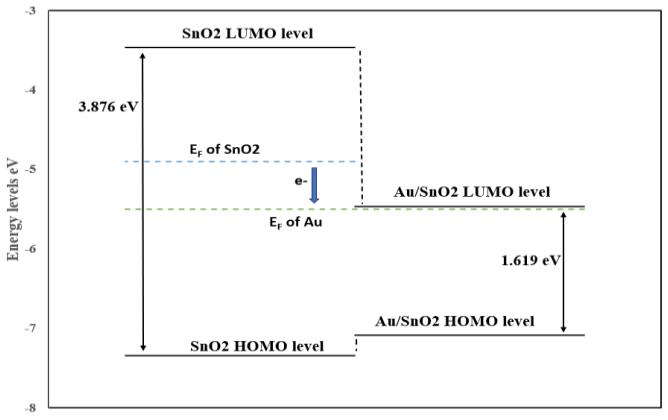

Figure. 8:. Energy gap, HOMO, and LUMO levels of pure and Au-doped SnO_2. Fermi levels of SnO_2 [27] and Au [28] are shown.

Table 1 lists the parameters that describe the present calculation of pristine and Au-doped SnO_2 clusters. As can be seen from Table 1, the unit of (A) is different in the two cases of H_2 and O_2 due to different temperature dependence exponent (m). As expected, the Gibbs free energy of transition of the Au-doped SnO_2 cluster is slightly lower than that of pristine SnO_2. The three values of $\Delta G^{\ddagger}$ are less than 0.1 eV since H_2 and O_2 are homomolecules with no dipole moments. However, a small, induced dipole moment is established in the two molecules as they approach pure and doped SnO_2 pyramids.

Table 1: Parameters used to simulate H_2 gas sensing and O_2 recovery model. $\Delta G^{\ddagger}$ values are at temperature 25 ℃ and normal pressure. An underscore is added to the oxygen in the third reaction to indicate an oxygen-deficient cluster.

No.	Reaction	A	$\Delta G^{\ddagger}$ (eV)	C (s)	m
1	$[SnO_2\text{---}H_2]^{v} \rightarrow [SnO_2\text{---}H_2]^{\ddagger}$	$3.7\ 10^{-9}\ s^{-1}.K^{-4}$	0.0623	80	4
2	$[Au/SnO_2\text{---}H_2]^{v} \rightarrow [Au/SnO_2\text{---}H_2]^{\ddagger}$	$1.6\ 10^{-9}\ s^{-1}.K^{-4}$	0.0586	47000	4
3	$[Au/Sn\underline{O}_2\text{---}O_2]^{v} \rightarrow [Au/Sn\underline{O}_2\text{---}O_2]^{\ddagger}$	$1.05\ s^{-1}$	0.0502	-	0

Conclusions

Theoretical modeling of H_2 gas reaction with pristine and Au-doped SnO_2 pyramid cluster is performed. The ambient O_2 reaction with the same clusters is also calculated, which corresponds to the recovery phase in a gas sensor system. A modified Evans–Polanyi principle is used to evaluate the Gibbs transition energy. The reaction of H_2 with oxygen in the air is accounted for using a logistic function. The calculated temperature variation of response, response time, and recovery time show that H_2 reactions increase with the fourth temperature power. In contrast, the O_2 recovery is dependent on temperature variation of Gibbs free energy of activation only. The theoretical results are all in acceptable agreement with the experiment.

Author contribution

Abdulsattar: All research activities.

Funding details

No funding was received.

References

1. A.G. Dana, M.S. Johnson, J.W. Allen, S. Sharma, S. Raman, M. Liu, C.W. Gao, C.A. Grambow, M.J. Goldman, D.S. Ranasinghe, R.H. West, W.H. Green, Automated reaction kinetics and network exploration (Arkane): A statistical mechanics, thermodynamics, transition state theory, and master equation software, International Journal of Chemical Kinetics. 55 (2023) 300–323. https://doi.org/10.1002/kin.21637.
2. L.P. Viegas, A Multiconformational Transition State Theory Approach to OH Tropospheric Degradation of Fluorotelomer Aldehydes, ChemPhysChem. 24 (2023). https://doi.org/10.1002/cphc.202300259.
3. I. Shefer, K. Lopez, A.P. Straub, R. Epsztein, Applying Transition-State Theory to Explore Transport and Selectivity in Salt-Rejecting Membranes: A Critical Review, Environmental Science and Technology. 56 (2022) 7467–7483. https://doi.org/10.1021/acs.est.2c00912.
4. M.A. Abdulsattar, The reaction of pristine and Rh-doped SnO2 clusters with acetone: Application of Evans–Polanyi principle to transition state theory, Journal of Molecular Modeling. 29 (2023). https://doi.org/10.1007/s00894-023-05710-5.
5. M.A. Abdulsattar, S.G. Khalil, T.H. Mahmood, Adsorption of Cl2 on pristine and Pd doped TiO2 clusters: A transition state theory study, Passer Journal of Basic and Applied Sciences. 5 (2023) 324–329. https://doi.org/10.24271/PSR.2023.403680.1339.
6. Y. Shang, Advanced kinetic calculations with multi-path variational transition state theory for reactions between dimethylamine and nitrogen dioxide in atmospheric and combustion temperature ranges, Physical Chemistry Chemical Physics. 25 (2023) 16824–16834. https://doi.org/10.1039/d3cp01336g.
7. Y. Kong, Y. Li, X. Cui, L. Su, D. Ma, T. Lai, L. Yao, X. Xiao, Y. Wang, SnO2 nanostructured materials used as gas sensors for the detection of hazardous and flammable gases: A review, Nano Materials Science. 4 (2022) 339–350. https://doi.org/10.1016/j.nanoms.2021.05.006.
8. Z. Li, W. Zeng, Q. Li, SnO2 as a gas sensor in detection of volatile organic compounds: A review, Sensors and Actuators A: Physical. 346 (2022). https://doi.org/10.1016/j.sna.2022.113845.
9. J. Bai, Y. Shen, S. Zhao, A. Li, Z. Kang, B. Cui, D. Wei, Z. Yuan, F. Meng, Room-Temperature NH3 Sensor Based on SnO2 Quantum Dots Functionalized SnS2 Nanosheets, Advanced Materials Technologies. 8 (2023). https://doi.org/10.1002/admt.202201671.
10. Y. Li, X. Song, L. Li, W. Wu, K. Tao, Z. Ying, Y. Hu, Y. Zhou, R. Zhang, G. Wang, F. Wen, Low concentration CO gas sensor constructed from MoS2 nanosheets dispersed SnO2 nanoparticles at room temperature under UV light, Ceramics International. 49 (2023) 10249–10254. https://doi.org/10.1016/j.ceramint.2022.11.204.
11. V. Mulloni, A. Gaiardo, G. Marchi, M. Valt, L. Vanzetti, M. Donelli, L. Lorenzelli, Sub-ppm NO2 Detection through Chipless RFID Sensor Functionalized with Reduced SnO2, Chemosensors. 11 (2023). https://doi.org/10.3390/chemosensors11070408.
12. S. Zhang, Y. Pu, S. Cao, D. Zhu, SnO2 Nanoparticles Derived from Metal-Organic Precursors as an Acetaldehyde Gas Sensor with ppb-Level Detection Limit, ACS Applied Nano Materials. 6 (2023) 13177–13187. https://doi.org/10.1021/acsanm.3c01917.
13. Z. Wang, Y. Wang, Impact of convection-diffusion and flow-path interactions on the dynamic evolution of microstructure: Arc erosion behavior of Ag-SnO2 contact materials, Journal of Alloys and Compounds. 774 (2019) 1046–1058. https://doi.org/10.1016/j.jallcom.2018.10.022.
14. L. Zhang, C. Jia, F. Bai, W. Wang, S. An, K. Zhao, Z. Li, J. Li, H. Sun, A comprehensive review of the promising clean energy carrier: Hydrogen production, transportation, storage, and utilization (HPTSU) technologies, Fuel. 355 (2024). https://doi.org/10.1016/j.fuel.2023.129455.
15. J. Wang, Y. Liang, Z. Zhao, Effect of N2 and CO2 on explosion behavior of H2-Liquefied petroleum gas-air mixtures in a confined space, International Journal of Hydrogen Energy. 47 (2022) 23887–23897. https://doi.org/10.1016/j.ijhydene.2022.05.152.
16. P. Wang, H. Zhang, S. Wang, J. Li, Controlling H2 adsorption of Cu/ZnO/Al2O3/MgO with enhancing the performance of CO2 hydrogenation to methanol at low temperature, Journal of Alloys and Compounds. 966 (2023). https://doi.org/10.1016/j.jallcom.2023.171577.
17. B.G. Ershov, A. V. Gordeev, Modeling the effect of O2 and H2 on the concentration of radiolysis products in the primary coolant of a VVÉR-440, Atomic Energy. 74 (1993) 109–113. https://doi.org/10.1007/BF00760350.
18. Hydrogen autoignition temperature, (n.d.). https://www.wolframalpha.com/input/?i=hydrogen+autoignition+temperature (accessed December 23, 2023).
19. A. Kanzariya, S. Vadalkar, S.K. Jana, L.K. Saini, P.K. Jha, An ab-initio investigation of transition metal-doped graphene quantum dots for the adsorption of hazardous CO2, H2S, HCN, and CNCl molecules, Journal of Physics and Chemistry of Solids. 186 (2024). https://doi.org/10.1016/j.jpcs.2023.111799.
20. C. Zhang, X. He, Y. Zhou, J. Xu, Z. Zheng, Y. Bian, M. Debliquy, Highly sensitive and stable yolk-shell Bi2MoO6 gas sensor for ppb-level isopropanol detection, Sensors and Actuators B: Chemical. 401 (2024). https://doi.org/10.1016/j.snb.2023.135059.
21. F. Arablouye Moghaddam, M. Babazadeh, E. Vessally, E. Ghasemi, S. Ahmadizadeh Shendy, An efficient HCN gas sensor by functionalized, decorated, and doped carbon nanocone strategy: A theoretical study, Inorganic Chemistry Communications. 156 (2023). https://doi.org/10.1016/j.inoche.2023.111118.
22. S. Killa, L. Cui, E.P. Murray, D.S. Mainardi, Kinetics of nitric oxide and oxygen gases on porous Y-stabilized ZrO 2-based sensors, Molecules. 18 (2013) 9901–9918. https://doi.org/10.3390/molecules18089901.
23. Y. Chen, K.H. Chang, F.Y. Meng, S.M. Tseng, P.T. Chou, Broadening the Horizon of the Bell–Evans–Polanyi Principle towards Optically Triggered Structure Planarization, Angewandte Chemie - International Edition. 60 (2021) 7205–7212. https://doi.org/10.1002/anie.202015274.
24. M.J. Frisch, G.W. Trucks, H.B. Schlegel, G.E. Scuseria, M.A. Robb, J.R. Cheeseman, G. Scalmani, V. Barone, B. Mennucci, G.A. Petersson, H. Nakatsuji, M. Caricato, X. Li, H.P. Hratchian, A.F. Izmaylov, J. Bloino, G. Zheng, J.L. Sonnenberg, M. Hada, M. Ehara, K. Toyota, R. Fukuda, J. Hasegawa, M. Ishida, T. Nakajima, Y. Honda, O. Kitao, H. Nakai, T. Vreven, J.A.J. Montgomery, J.E. Peralta, F. Ogliaro, M. Bearpark, J.J. Heyd, E. Brothers, K.N. Kudin, V.N. Staroverov, R. Kobayashi, J. Normand, K. Raghavachari, A. Rendell, J.C. Burant, S.S. Iyengar, J. Tomasi, M. Cossi, N. Rega, J.M. Millam, M. Klene, J.E. Knox, J.B. Cross, V. Bakken, C. Adamo, J. Jaramillo, R. Gomperts, R.E. Stratmann, O. Yazyev, A.J. Austin, R. Cammi, C. Pomelli, J.W. Ochterski, R.L. Martin, K. Morokuma, V.G. Zakrzewski, G.A. Voth, P. Salvador, J.J. Dannenberg, S. Dapprich, A.D. Daniels, Ö. Farkas, J.B. Foresman, J. V. Ortiz, J. Cioslowski, D.J. Fox, Gaussian 09, Revision D.01, (2013).
25. M.A. Abdulsattar, GaxIn2-xO3 surface pyramids interaction with formaldehyde: thermodynamic and sensing analysis, Karbala International Journal of Modern Science. 9 (2023) 8. https://doi.org/10.33640/2405-609X.3324.
26. X.T. Yin, L. Tao, Fabrication and gas sensing properties of Au-loaded SnO2 composite nanoparticles for low concentration hydrogen, Journal of Alloys and Compounds. 727 (2017) 254–259. https://doi.org/10.1016/j.jallcom.2017.08.122.
27. L. Guo, Z. Shen, C. Ma, C. Ma, J. Wang, T. Yuan, Gas sensor based on MOFs-derived Au-loaded SnO2 nanosheets for enhanced acetone detection, Journal of Alloys and Compounds. 906 (2022). https://doi.org/10.1016/j.jallcom.2022.164375.
28. C. Kittel, Introduction to Solid State Physics, 5th ed., John Wiley and Sons Inc., New York, 1976.